Design and performance of flexible polymeric piezoelectric energy harvesters for battery-less tyre sensors

OPEN ACCESS
IOP Publishing
Smart Materials and Structures
Smart Mater. Struct. **31** (2022) 095034 (15pp)
https://doi.org/10.1088/1361-665X/ac8211

Design and performance of flexible polymeric piezoelectric energy harvesters for battery-less tyre sensors

Carmela Mangone[1,2,*], Wisut Kaewsakul[1,*], Michel Klein Gunnewiek[2], Louis A E M Reuvekamp[1,2], Jacques W M Noordermeer[1] and Anke Blume[1]

[1] Elastomer Technology and Engineering (ETE), Department of Mechanics of Solids, Surfaces and Systems, Faculty of Engineering Technology, University of Twente, P.O. 217, Enschede, 7500 AE, The Netherlands
[2] Apollo Tyres Global R&D, Colosseum 2, Enschede, 7521 PT, The Netherlands

E-mail: c.mangone@utwente.nl and w.kaewsakul@utwente.nl

Received 22 March 2022, revised 8 July 2022
Accepted for publication 17 July 2022
Published 3 August 2022

Abstract

A piezoelectric energy harvester for battery-less tyre sensors has been developed. It consists of two key elements: (a) a piezoelectric material—polyvinylidene difluoride (PVDF) film and (b) an electrode—a conductive elastomer filled with carbon black and single-wall carbon nanotubes (SWCNTs). It was designed as a flexible patch in a sandwich-like configuration, which can be mounted onto the inner liner of a tyre. The patch was fabricated by inserting a PVDF film in between two conductive elastomer sheets. The development started with improving the conductivity of the elastomer by adding 6 wt% of SWCNT masterbatch. The adhesion between the interfaces was improved through surface modification of the PVDF film by introducing oxygen functional groups via a plasma treatment and further modification with a thiocyanate silane. The successful surface modification of the PVDF film was affirmed by x-ray photoelectron spectroscopy. T-peel and fatigue tests showed durable and stable adhesion between PVDF and conductive elastomer, confirming that the silane can effectively bridge the two components. A glueing method is proposed to adhere the patch to the tyre inner liner compound. The harvester is estimated to sufficiently power a reference tyre sensor, producing 28 μW cm^{-2}.

Keywords: piezoelectric energy harvester, self-powered systems, piezoelectric polymer, conductive elastomer

(Some figures may appear in colour only in the online journal)

* Authors to whom any correspondence should be addressed.

1. Introduction

Over the last decades, energy-harvesting systems have received growing attention for their unique potential in enabling battery-less sensors and self-powered operations [1, 2]. Energy harvesters are capable of deriving energy from environmental sources, like heat, solar light or mechanical vibrations. The obtainable energies can be converted into a useable form as electrical power. These self-generating electricity systems can function as power sources for electronic devices, mitigating the disadvantages associated with the use of batteries, such as the limited lifetime of such a device due to emptied energy, environmental pollution, and undesired high maintenance costs.

The automotive industry is one of the most profitable stakeholders of this energy-harvesting technology [3, 4]. The rapid development of autonomous and electric driving results in the use of multiple sensors installed in vehicles. A good example of such sensor systems is a tyre pressure monitoring system (TPMS) mounted in car tyres. This device is growing in use to monitor the conditions of tyres while running. The online data derived from the TPMS can be used to evaluate the tyre performances, e.g. fuel consumption efficiency and safety aspects according to the regulations established in Europe, the US and Asia [5]. A TPMS system can indicate whether the running tyres are under- or over-inflated by monitoring the real-time pressure of the tyres. Attempts to further improve the TPMS features are continuously made [6, 7]. Therefore, developing a self-powered TPMS is highly attractive for this advancement.

Various energy harvesters have evolved for powering autonomous TPMSs [8–11]. Among those, piezoelectric energy harvesters (PEHs) are highlighted as the most suitable technique. This technology includes a piezoelectric material placed between two electrodes. Upon externally applied mechanical forces, electrical charges are accumulated on both sides of the piezoelectric material and therefore, the electrodes induce a flow of electrical current. This mechanism may be employed within the operating conditions of car tyres. When a tyre is in contact with the road surface, it is continuously subjected to dynamic mechanical excitations involving externally applied forces, deformations, temperatures, as well as varied vibrations during rotating. The repetitious deformations of the piezoelectric materials, when installed as a part of a tyre at an appropriate position, provide the potential to continually produce electricity that can then be stored in the capacitor of a TPMS [11].

A variety of PEHs has been proposed to be fabricated for powering such sensors in tyres; different categories of piezoelectric materials were previously investigated and reported in the literature [4, 8, 10–14]. Several studies proposed multiple designs of piezoelectric ceramic disks with a metal electrode mounted in tyres, which were able to generate the electrical power over a wide range of running speeds of a tyre, 30–180 km h^{-1} [15–17]. In all cases, the designs fulfilled the reliability and cost requirements. However, the use of a metal electrode was a major disadvantage, due to large acceleration shocks. Later, the use of bump stops was suggested as a solution to limit the vibration amplitude and to maintain the structural integrity of the harvesters [18]. The use of a bump stop decreased the maximum bending stress generated on the harvesters but tended to reduce the generated power. Other researchers investigated the use of an elastomeric material to attach the piezoelectric disk on a tyre wheel, and the configuration of a harvester was mounted perpendicular to the tyre tread inner-wall surface [19, 20]. For the first case, the piezoelectric ceramic based on lead zirconium titanate (with formula $PbZr_{0.58}Ti_{0.42}O_3$: PZT) survived for only 10 min when an endurance test was carried out at 60 km h^{-1}. In the second case, a cantilever PZT with dimensions of 70 × 7 × 0.32 mm produced 500 μW at 50 km h^{-1}, but it was reported to be difficult to install the PEH in a configuration perpendicular to the tyre tread area. In 2012, Makki and Pop-Iliev [21, 22] made a comparison between a piezoelectric ceramic PZT and polymer—polyvinylidene difluoride (PVDF) by applying both materials to the inner liner of a tyre. The PZT disk with a thickness of 0.23 mm produced a higher value of electrical power, i.e. 4.5 mW, compared to a PVDF film with a thickness of 0.11 mm and a lateral dimension of 40 × 40 mm that gave only 0.85 mW. Nevertheless, the authors concluded that the higher flexibility of PVDF is advantageous over piezoelectric ceramics, limited in terms of rigidity and interfacial adhesion. This flexibility leads to a longer lifetime and good performance under dynamic applications [23–25].

From the literature described above, the use of a metal electrode does not lead to the best performance of a PEH when applied to a rolling tyre. Extensive investigations have been conducted to find the replacements for flexible electrodes, such as graphenes [26, 27], metal nanowires [28, 29], conductive inks [29, 30]. Appraising among these candidates to be applied for flexible electronics, electrically conductive elastomers are the most promising alternative due to their elastic nature and the ease of mounting into the tyre. Generally, elastomers are insulating materials because their molecules are hydrocarbons with single carbon–carbon bonds along their polymeric chains, which do not allow delocalization of electrons between atoms and the transfer of electrical current [31]. Introducing carbon black (CB) particulates in the elastomeric matrix can create a continuous particles network, through which electrons are transferred [31, 32]. Hence, the formation of such CB particulates network can establish electrical conductive pathways within an elastomer matrix.

In the present study, a piezoelectric polymer and an electrically conductive elastomer were investigated as components of a flexible PEH able to withstand tyre rolling conditions. Among polymer materials, β-PVDF is the most investigated candidate for energy harvesting due to its high piezoelectric coefficient and stability. Elastomeric electrodes were then selected to ensure maintaining the structural integrity of the elastomer under tyre rolling conditions. Conductive particles, such as CB and single-wall carbon nanotubes (SWCNTs), were incorporated into this elastomeric phase to enhance its electrical properties. The PEH prototype in the current study was designed as a sandwich configuration, based on a PVDF film inserted in between two layers of an elastomeric

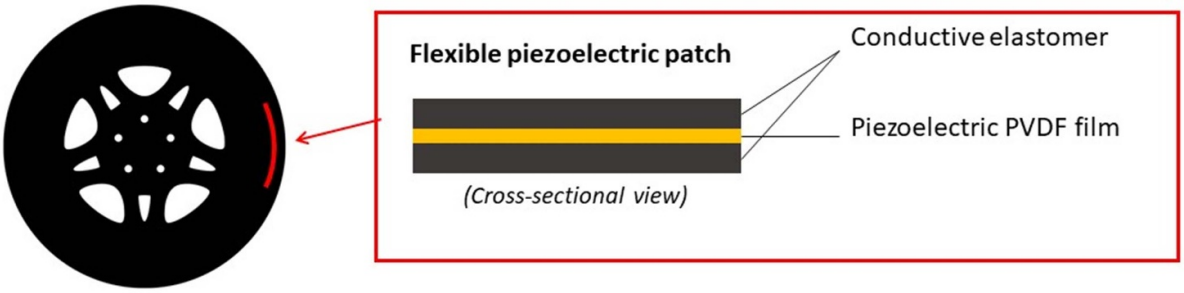

Figure 1. Conceptual design of piezoelectric energy harvester proposed in this study.

conductive compound. To fabricate this PEH, there are crucial developing procedures involved, like enhancing the electrical conductivity of the elastomeric layers and energy generation of the piezoelectric polymer, achieving sufficient adhesion of both components as well as to the inner liner of a tyre. Additionally, measurements are conducted to validate the performance of a resulting prototype in tyre rolling conditions. The design concept and methodologies to optimise and validate the component materials and the final prototype are described in this manuscript. The resulting harvester patch is finally verified to substantiate if the output electrical power can sufficiently support a reference TPMS sensor.

2. Conceptual design

The PEH in this study was developed through several steps. As it should be attached to the inner liner of tyres, it needs to tolerate the dynamic operational conditions of the rolling tyres, which involves variable parameters, i.e. loads, strains, and temperatures. Thus, the compatibility and the adhesion between these two components must be sufficient, so that the designed prototype can withstand these harsh dynamic conditions. For this design system, the piezoelectric harvester needs to generate a sufficient amount of electricity of approximately 28 mW to power a TPMS sensor [4]. The conductive compound needs to have adequate conductivity of around 10^{-5}–10^{-2} S cm^{-1}, to ensure that the desired amount of generated electricity can be transported to the TPMS device [31]. In addition, safety, reliability and cost should also be taken into consideration.

Regarding the aforementioned requirements, the PEH was designed as a sandwich configuration consisting of two key elements, as shown in figure 1: a piezoelectric polymer β-PVDF film constructed in between two layers of a conductive elastomeric compound. PVDF is a semi-crystalline polymer with repeating units (CH_2–CF_2). Among the four crystalline polymorphic phases, β-PVDF is piezoelectric due to the presence of a dipole moment induced by an all-trans planar conformation. When an external load is applied, dielectrics of the material are deformed and equal, opposite charges are generated on the film surface. The conductive compound applied on each side of the material induces the flow of the charge carriers. The conductive compound is an elastomer filled with conventional reinforcing CB and SWCNTs.

According to the design concept, the project is divided into four steps:

- Preliminary tests of separate components by measuring the electrical properties of the piezoelectric polymer PVDF film and the elastomeric conductive compounds;
- Verifying and improving the conductive and piezoelectric properties of the selected materials under dynamic deformations simulating tyre rolling conditions;
- Evaluation of the PEH regarding the adhesion of the key system elements and output power under tyre rolling conditions;
- Investigation of the adhesion performance between the PEH and the inner liner of a tyre.

Validation of the design is the final development step that primarily confirms the feasibility of the application in a pragmatically operational situation.

3. Experimental

3.1. Materials

The piezoelectric polymer PVDF was supplied by PolyK Technologies LLC (Philipsburg, USA) in the form of a 100 μm thin film with A4 size. The electrical and chemical properties of this polymer film are given in table 1. The PVDF surface was cleaned by chloroform (99.5%, Sigma-Aldrich, St. Louis, MO, USA), treated with an oxygen plasma and silanised with a thiocyanate-based silane coupling agent: 3-thiocyanatopropyltriethoxysilane (Si-264, Evonik Industries AG, Essen, Germany). The physical and chemical properties of 3-thiocyanatopropyltriethoxysilane are reported in table 2.

The reference compound C_{ref} included three rubber types: natural rubber (NR, TSR 20), high-cis branched butadiene rubber (BR 1280) and styrene BR (SBR 1502). The CB employed was N330 with its specific surface area brunauer-emmett-teller or (BET) method, ASTM D-6556) and structure values oil absorption number (OAN) method, ASTM D-2414) of 78 m^2 g^{-1} and 88 ml/100 g, respectively. Rubbers, CB, processing oil, curing agents and anti-degradants of C_{ref} compound were supplied by Apollo Tyres Global R&D Ltd. The conductivity of C_{ref} was further improved by adding highly conductive SWCNTs, 10 wt% dispersed in a low aromatic

Table 1. Properties of the PVDF film with 100 μm thickness.

Properties[a]	Values
Charge coefficient, d_{31}	30 pC N^{-1}
Charge coefficient, d_{33}	-30 pC N^{-1}
Glass transition temperature	-34 °C
Melting temperature	170 °C–175 °C
Curie temperature	100 °C
Tensile strength	400–600 MPa
Young's modulus	2300 MPa
Elongation at break	20%–30%

[a] From PolyK Technologies LLC, USA.

Table 2. Physical and chemical properties of 3-thiocyanatopropyl triethoxysilane (Si-264).

Properties[a]	Values
Sulphur content	12.5%
Average molecular weight	263 g mol^{-1}
Density	1.00 g cm^{-3}

[a] From Evonik Industries AG.

Table 3. Compositions of conductive rubber compounds.

	Amount (phr)			
Ingredients	C_{ref}	C_1	C_2	C_3
NR, TSR-20	25	25	25	25
SBR 1502	25	25	25	25
BR 1280	50	50	50	50
CB N330	60	60	60	60
Processing oil	14	14	14	14
Curing agents	10	10	10	10
Anti-degradants	7	7	7	7
SWCNT/TDAE	0	4	8	12

plasticizer, treated distillate aromatic extract or TDAE oil, as masterbatch Matrix 603 (OCSiAl Europe, Luxemburg). Three compounds were prepared with 2, 4 and 6 wt% of the SWCNT masterbatch, coded C_1, C_2 and C_3, respectively. Table 3 shows the compositions of the C_{ref}, C_1, C_2 and C_3 compounds.

To investigate the possible application of the piezoelectric harvester in a tyre, the adhesion of the system towards an inner liner was investigated. The compound used for the inner liner was provided by Apollo Tyres Global R&D Ltd, coded C_{IL}. The piezoelectric system was co-cured or glued to the vulcanised inner liner using an amine-silicone sealant: Teroson SI 33 from Henkel AG & C (Düsseldorf, Germany).

3.2. Sample preparation

3.2.1. Preparation of the conductive elastomeric compounds. The compounds C_1, C_2 and C_3 were prepared by adding 2, 4 and 6 wt% of the SWCNT/TDAE masterbatch to C_{ref} on a two-roll mill for 7 min and 2 mm nip width (Polymix 80 T, Schwabenthan-Maschinen GmbH & Co. KG, Berlin, Germany). To obtain a good dispersion level of the nanofillers, the compound C_{ref} mixed with the required amount of SWCNT/TDAE masterbatch was passed through the two-roll mill ten times. To vulcanise the conductive rubber samples, the vulcanisation characteristics of the compounds were analysed using a Rubber Process Analyser (RPA 2000, Alpha Technologies, Ohio, USA). Each measurement was done for 40 min at 140 °C at a frequency of 1.667 Hz and a strain amplitude of 0.5°. The optimum vulcanisation time, i.e. the time when the cure torque reaches 90% of its maximum, known as t_{c90}, was taken as input for the vulcanisation. The compounds were cured at 100 bar in a Wickert press WLP 1600 (Wickert Maschinenbau GmbH, Landau, Germany) to their t_{c90} at 140 °C. The samples obtained had a cylindrical shape with a diameter of 10 mm and a thickness of 4 mm.

3.2.2. Preparation of the piezoelectric harvesters. Surface modification of the piezoelectric PVDF film was carried out to improve the interfacial adhesion between the PVDF film and the elastomeric conductive compounds. First, the PVDF film was treated with an oxygen plasma method using a Plasma-Prep II (SPI Supplies, West Chester, Pennsylvania, USA) consisting of a plasma vacuum chamber, in which the PVDF film was placed. A mechanical vacuum pump (Oerlikon, Lafert S.p.A., Piave, Italy) reduced the pressure inside the chamber to around 100–200 mTorr. After reaching this optimal pressure, oxygen gas was led into the chamber. A radio-frequency power at 13.56 MHz was applied to the chamber to excite and charge the oxygen molecules by turning them in oxygen radicals. The film was treated with this oxygen plasma for 15 min at room temperature. After this stage, the PVDF film surface had been randomly covered with hydroxyl and carbonyl groups which are highly reactive towards the subsequent treatment step known as 'silanisation'. The silanisation of the oxygen-treated PVDF film was carried out using the silane coupling agent 3-thiocyanatopropyltriethoxysilane. For this, the plasma-treated film was introduced into a desiccator under vacuum at room temperature for 1 or 24 h. Inside the desiccator, the film was fixed with a holder to fully expose the surface of the film to the silane vapour. About 3 ml of 3-thiocyanatopropyltriethoxysilane silane in a small Petri dish was placed close to the film.

The chemical structure of the modified PVDF film surface was characterised and confirmed for its modification efficacy using x-ray photoelectron spectroscopy (XPS) (PHI Quantera SXM, Chanhassen, Minnesota, USA). The PVDF films were irradiated using a monochromatic x-ray beam (Al Kα, 1486.6 eV) with a spot size of 100 μm. The XPS measurements were performed after each step of the surface treatment, i.e. after the oxygen plasma modification and after the silanisation at two different reaction times—1 and 24 h. The two reaction times were applied to verify which reaction time was adequate. Each spectrum was compared with the spectrum of a pure PVDF film cleaned before the analysis using chloroform. All samples were analysed at four different spots to confirm the evenness of the modification over the films.

After the silane treatment, the PVDF films were assembled with the conductive compound sheets. This sandwich design

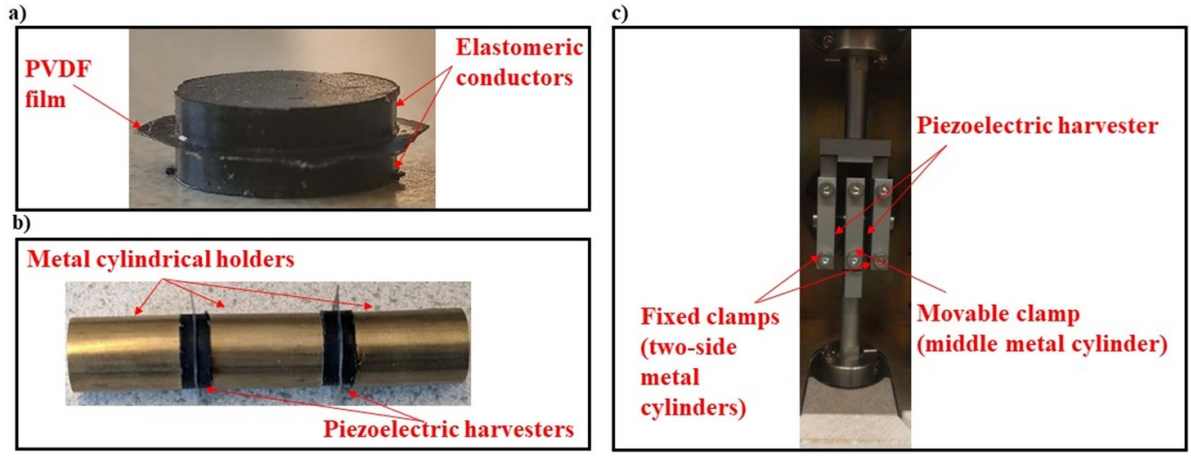

Figure 2. Configurations of a sandwich-like piezoelectric harvester (a); a double shear specimen from two piezoelectric harvesters glued in between three metal holders (b); and the double shear clamp of the DMA (c).

was cured into the desired cylindrical shape using compression moulding in the Wickert press WLP 1600 at 100 bar to its t_{c90}. The applied curing temperature of the piezoelectric sandwich is highly important. This is because, at around 100 °C which is the so-called Curie temperature of the PVDF, a transition from β-PVDF to δ-PVDF takes place. This reorientation of the β-dipoles results in the depolarization of the polymer, leading to a decrease in piezoelectric performance [33]. Therefore, the effect of the curing temperature was investigated, as the PVDF film and conductive elastomers were assembled into a sandwich design (figure 1) by co-curing them at three different temperatures, i.e. 120 °C, 140 °C and 160 °C.

The piezoelectric patch was fabricated into a sandwich configuration with a 0.1 mm thick PVDF film inserted in between the two sheets of a 2.0 mm thick conductive compound. Thus, a piezoelectric patch with about 4.1 mm thickness was achieved. In figure 2(a), the final piezoelectric patch is shown.

3.3. Sample characterisations

3.3.1. Adhesion between PVDF film and conductive compound. The adhesive strength between the PVDF film and elastomeric conductive compound was investigated using a T-peel test. The measurement was performed in a tensile machine (Zwick Z1.0, Zwick/Roell, Venlo, the Netherlands) according to the ASTM D413 test standard. The specimen includes the PVDF film (with and without surface modification), a 2 mm thick reference compound C_{ref} and a 0.1 mm thick cotton fabric cloth (Twentse Damast Linnen en Katoenfabriek B.V., Losser, the Netherlands). The layers were cured into the desired tensile sheet at 100 bar using compression moulding in the Wickert press WLP 1600 to their t_{c90} at 140 °C. The dimensions of the obtained specimen were 20 mm in width and 120 mm in length. The cotton fabric cloth was inserted on the external side of the conductive compound so that the adhesion strength will not be influenced by this large deformation of the elastomer during the test. After having mounted the two components into the two 20 mm distant fixtures of the tensile machine, the two components were peeled apart at a constant rate of 20 mm min^{-1}. The adhesive strength needed to separate the virgin and surface modified PVDF from the reference conductive compound was measured. Five samples were tested and the data were averaged.

The adhesion bond stability between the two components, i.e. the PVDF film and the conductive elastomeric compounds, was investigated using a Dynamic Mechanical Analysis DMA Eplexor 9 (Netzsch Gabo Instruments GmbH, Ahlden, Germany) with a time sweep measurement. Two piezoelectric sandwich patches (prepared according to the procedure described in section 3.2.2) were glued using a cyanoacrylate adhesive, i.e. Sicomet 7000 (Henkel AG & C, Düsseldorf, Germany), to three metal cylindrical sample holders forming a double shear specimen (see figure 2(b)). Then, the specimen was placed in the double shear clamp of the dynamic mechanical analyser (DMA) (figure 2(c)). The two side-cylinders were fixated in the clamp and not movable, while the oscillating force acts on the middle cylinder which is the movable position. The time sweep test was performed at 10 Hz, room temperature, 2% of dynamic strain, for 20 h. This measurement was also applied for validating the adhesion performance between the inner liner and the conductive compound. The conductive rubber sheet and the inner liner were separately cured into a thickness of 2 mm at 140 °C and 180 °C, respectively. Afterwards, these two components were prepared into a small cylinder with a diameter of 10 mm and then glued together by the silicon adhesive, i.e. Teroson Si 33. Finally, the glued rubber parts were adhered to the metal cylinders for a double shear analysis using Sicomet 7000 cyanoacrylate adhesive. To quantify the repeatability, three samples were measured individually prepared by assembling conductive compounds from the same masterbatch with PVDF films subjected to surface modification in one batch. The same for the adhesion of conductive compound and inner liner, three samples from the same masterbatch were vulcanised and measured.

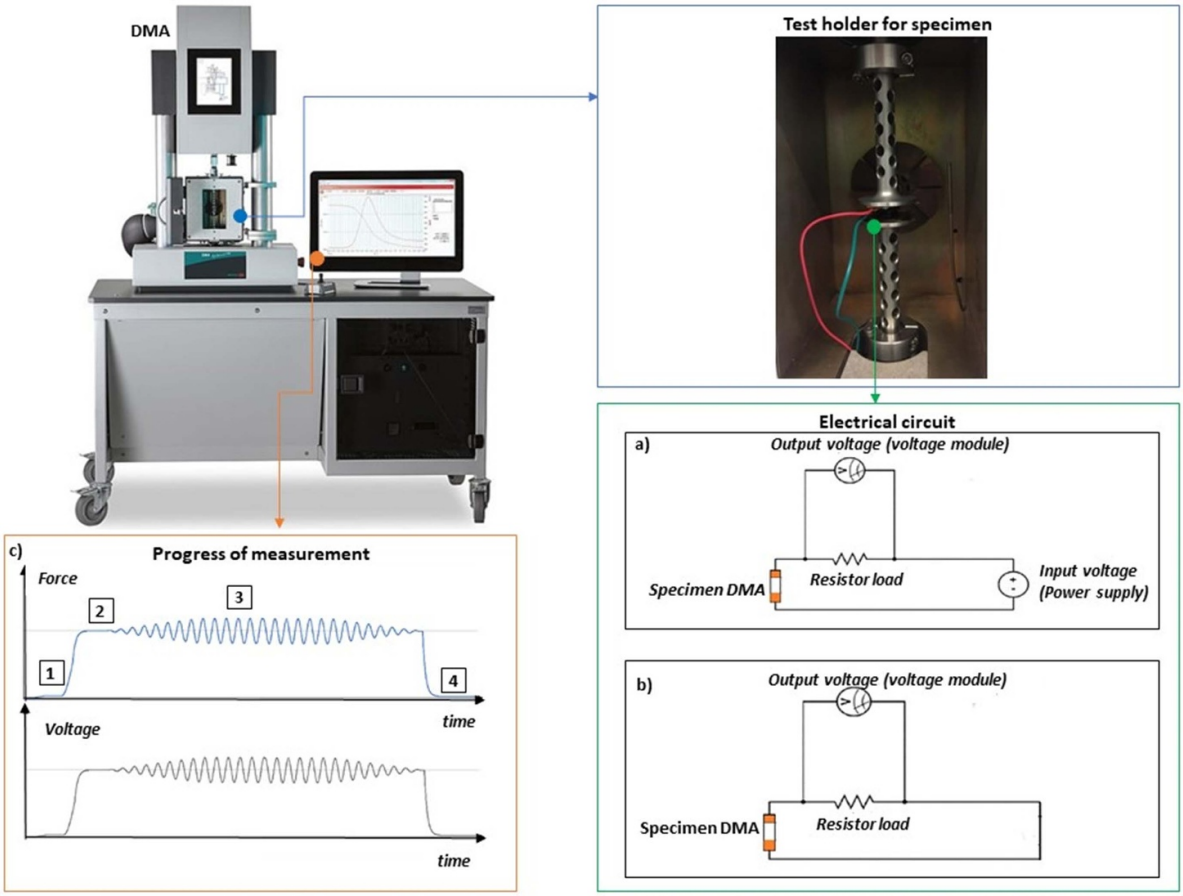

Figure 3. Schematic view of the in-house measurement setup: DMA with test holder for the specimen in compression mode coupled to the electrical circuit for conductive (a) and piezoelectric measurements (b). Progress of the measurements as an example (c).

3.3.2. Setup for electro-dynamic mechanical measurements. The conductivity and piezoelectricity of the investigated materials were characterised using in-house developed setups. They consisted of a DMA to simulate the dynamic mechanical conditions of running tyres. The DMA used in this work was the DMA Eplexor 9. The measurements were performed in compression mode in two modalities: with varying temperatures in the range from 0 °C to 100 °C at set frequencies of 10 and 100 Hz; with varied frequencies from 1 to 100 Hz at 20 °C. Concerning the electrical properties, the voltage was measured under dynamic mechanical conditions simulated by the DMA. To measure the electrical conductivity or piezoelectricity of the materials, copper plates with electrical wires were attached to the upper and lower parts of the specimen to create a connection with the electrical measuring devices. The attachment of the copper plates to the compression clamp of the DMA is shown in figures 3(a) and (b). To avoid an electrical shortcut, a specimen needs to be isolated from the metal clamps which were therefore covered with Kapton tape, i.e. polyimide (PrintTec, Geldermalsen, the Netherlands).

The dynamic analyses were developed based on the assumption of a certain car, selected as an example by taking into account its weight and tyre series typically used for this car [34]. Hence, the applied load on each tyre was estimated and the analysis conditions were simulated. To quantify the repeatability of these dynamic analyses, three samples were again measured individually prepared by assembling conductive compounds from the same masterbatch with PVDF films subjected to surface modification in one batch.

The electrical conductivity of the elastomeric compounds was determined by applying a specific current, where the voltage between two metal probes attached to both ends of the conductive compounds was measured. The measurement setup included a direct current (DC) power supply (0–30 V, 3 A, TENMA, Farnell House, Leeds, UK) to apply an electrical current to the specimen and a voltage module (Model NI-9215, National Instruments, Austin, TX, USA) to monitor the corresponding voltage drop over a shunt resistor placed in series with the specimen. A shunt circuit is used to divert a small part of the current flow and to detect the current across the circuit. Thereby, the conductivity of the specimen is calculated. A compact-DAQ chassis (Model cDAQ-9171, National Instruments, Austin, TX, USA) connects the module to a USB port and, in turn, records the changes in voltage using computing software. In figure 3(a) the electrical circuit for the conductive measurements is demonstrated.

Figure 3(c) is a typical example of a simultaneous registration of the applied dynamic force and the resulting voltage at

a particular combination of parameters settings. After having applied the contact force (point 1 in figure 3(c)) and the static and dynamic loads (points 2 and 3), the resulting voltage followed the same path [35]. This measured voltage was used to calculate the electrical conductivity, which is expressed by the following equation [36]:

$$\sigma = \frac{(V_{PS} - V_s)}{I_s}\frac{l}{A_i} = \frac{R(V_{PS} - V_{out})}{V_s}\frac{l}{A_i}. \quad (1)$$

The voltage-drop over the sample is the difference between the voltage from the power supply (V_{PS}) (4 V for the tests) and the one measured by the voltage module (V_S). The current I_s was calculated using Ohm's law by inserting the voltage output from the specimen and the value of the resistor (1 MΩ). The DMA registered the distance l between the electrodes while the cross-sectional area A_i is calculated by taking into account the cylindrical shape of the specimen, i.e. 10 mm diameter.

With the same concept as the conductivity measurement setup, the output voltage generated by the piezoelectric patch was monitored. For this setup, the electrical circuit was simplified: figure 3(b). It included a shunt resistor placed in series with the specimen to divert the generated current flow by the specimen across the voltage module. The PVDF film in a piezoelectric patch produces electrical charges that move to the patch surface. Then, the conductive elastomer layers help to transport the generated electrical current to a voltage module, used to monitor the output voltage. The application of sinusoidal stresses to the piezoelectric patch leads to sinusoidal voltages as well due to the generation of alternating current (AC). The power output (P, μW cm^{-2}) of the piezoelectric patch is calculated using equation (2) [37]:

$$P = \frac{\langle V^2 \rangle}{R}\frac{1}{\text{Instantaneous cross sectional area}}(\mu\text{W cm}^{-2}) \quad (2)$$

where $<V^2>$ is the average of the squared generated voltage in the dynamic phase while the cross-sectional area is calculated taking into account the cylindrical shape of the specimen. The maximum amount of power is reached when the resistor is balanced to the internal resistance of the piezoelectric patch. The maximum power was obtained with a resistor of 4.7 MΩ. Therefore, this value was used for further analysis.

4. Results and discussion

4.1. Measuring parameters based on a reference car

The analysis of the material conductivity and piezoelectricity was performed according to the actual conditions of a rolling tyre. The DMA analysis was used to simulate these conditions, by selecting a proper value of temperature, frequency and deformation. During car driving, the temperature inside a tyre can increase up to around 100 °C [38]. On the other side, conductive elastomers lose their conductivity in the region of the glass transition [35]. The compounds analysed in this study have a glass transition temperature at around −40 °C and the transition region ends at appr. 0 °C. Therefore, a temperature sweep analysis was performed in the range between 0 °C and 100 °C at 10 Hz, which is a rotational frequency of a car driving at a speed of 80 km h^{-1}.

Tyre-road interactions also contribute to vibrations in the tyre. The operating frequency varies in the range between 1 and 100 Hz [38]. Assuming as a reference a passenger tyre of the size 205/55R16 94R in Volkswagen Golf running at a speed of 80 km h^{-1}, the frequency due to tyre-road interactions is calculated via the following equation:

$$f = n \cdot \left[\frac{v\,(\text{km h}^{-1})}{C\,(\text{m}) \cdot 3.6}\right] \quad (3)$$

where n is the number of excitations per revolution and the term in the bracket is the rotations per second, v is the speed of the vehicle and C is the tyre circumference. Based on proprietary information, the order n was measured at 80 km h^{-1}, an average value of 10th order was selected. The circumference C of the selected tyre is 1.98 m. From these, the conductivity and piezoelectricity were measured in the frequency sweep from 1 to 100 Hz at room temperature.

The static and dynamic stresses applied for the measurements were based on the compression pressure under which the tyres are subjected during driving. Based on the assumed tyre size 205/55R16 94R with a total surface area A_{tyre} and the Volkswagen Golf with a total weight ($W_{vehicle}$) of 2100 kgf, the surface area of the tyre in contact with the road, the contact patch area ($A_{contact\ patch}$) is as follows:

$$A_{contact\ patch} = 7\%A_{tyre} = 0.029\text{m}^2. \quad (4)$$

The force F_{tyre} exerted on each tyre is calculated from the vehicle weight $W_{vehicle}$, the gravity constant g (9.81 m s^{-2}) and the number of tyres in a vehicle (i.e. four wheels), as follows:

$$F_{tyre} = \frac{W_{vehicle} \cdot g}{4} = 5150.25\,\text{N}. \quad (5)$$

The average pressure exerted on a tyre (P_{tyre}) by a car-load was calculated with the ratio between the forces exerted on the tyre and the surface area of the contact patch:

$$P_{tyre} = \frac{F_{tyre}}{A_{contact\ patch}} \approx 0.18\,\text{MPa}. \quad (6)$$

However, the tread pattern of the tyre includes 30% of voids, i.e. grooves; this means that only 70% of the tyre tread is in contact with the road surface. Thus, the average pressure exerted on the contact patch area ($P_{contact\ patch}$):

$$P_{contact\ patch} = \frac{P_{tyre}}{70\%} \approx 0.26\,\text{MPa}. \quad (7)$$

A static stress of 0.35 MPa was then selected for the electro-mechanical measurements when taking into account any possible extra loads from a driver, passenger(s) and carried luggage. The dynamic stress peak-to-peak was set at 0.25 MPa.

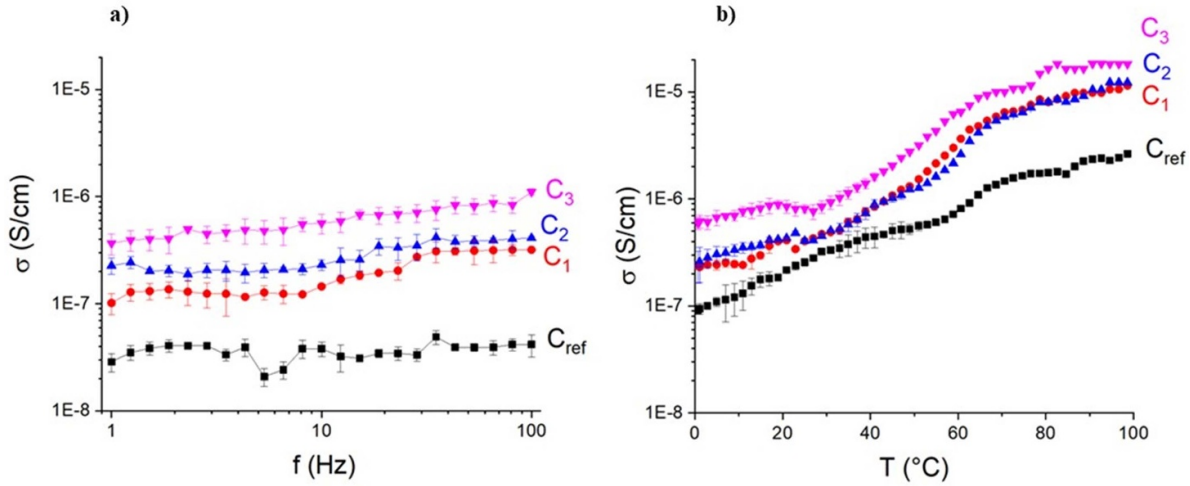

Figure 4. Electrical conductivity σ of the compounds C_{ref}, C_1, C_2 and C_3, analysed with static and dynamic stresses of 0.35 and 0.25 MPa, respectively; (a) with varying frequencies of 1–100 Hz at 20 °C; (b) varying temperatures from 0 °C to 100 °C at 100 Hz.

4.2. Conductive properties of elastomer compounds

The dynamic mechanical condition causes a periodic disruption of the filler network in the elastomeric sample due to the oscillating deformation, resulting in an alternating connection and disconnection of the filler particles. This concept was recently studied in detail by Bhagavatheswaran in his work in which the piezoresistive properties of elastomeric compounds under dynamic conditions and the relationship between dynamic mechanic analysis and electrical resistivity were studied [39]. In CB and carbon-nanotubes filled elastomers under dynamic strain, the filler network disrupts and recover harmoniously, increasing and decreasing the interparticle distance and causing the change in electrical conductivity over time. When applying subsequent cycles, the rearrangement of the filler network happens already in the first cycle, after which a stable response is observed. Therefore, the effect of consecutive cycles of a temperature sweep was investigated.

The electrical conductivity of the elastomeric compounds as a function of frequency is shown in figure 4(a). The use of carbon nanotubes improves the conductivity of the reference compound C_{ref}, in particular the compound C_3 with the 6 wt% of SWCNT masterbatch. Increasing the nanofiller concentration results in a denser filler network above the percolation threshold and closer distances between the filler particles, promoting denser conductive pathways in the material. The conductivity shows no frequency-dependent trend in case of C_{ref}, commonly called 'DC conductivity'. In contrast, it tends to increase with frequency for the compounds C_1–C_3, called 'AC conductivity'. In C_{ref}, filled with 60 phr of CB N330, a conductive path of CB particles is present and the conduction mechanism is due to an electrical tunnelling effect between close aggregates of the filler. The compounds C_1–C_3 contain joint conductive networks of CB and SWCNT. Therefore, the frequency-dependent conductivity of these compounds depends on the fact that the amount of SWCNT added is not high enough to form another conductive percolation network next to the one already existing based on the regular carbon black. This implies the existence of a regime in which the AC conductivity varies based on the diffusion of charge carriers in the fractal aggregates and obeys a power-law relationship. These results are in agreement with the results reported in literature [40, 41].

The electrical conductivity of all compounds as a function of temperature is depicted in figure 4(b). The compounds exhibit an enhanced conductivity by increasing the temperature from 0 °C to 100 °C. Elevated temperatures accelerate the charge carriers. This result is in good agreement with the observation from the frequency sweep analysis. It can be interpreted following the same concept of the higher extent of filler networks of conductive paths in the materials when a higher concentration of carbon nanotubes is applied. The increase in the conductivity with higher temperature seems to level off at a certain temperature as a result of lower volume density.

The results from the dynamic analysis using three consecutive temperature sweeps of the conductive compounds are shown in figure 5. The electrical conductivity of all vulcanisates increases with increasing measurement cycles due to orientation effect of the filler networks. The filler particles tend to align in longitudinal direction of the deformation, which is induced by the applied static and dynamic forces. This effect is also seen in figures 4(a) and (b) in which the values of the samples tested with the temperature sweep at 20 °C and 100 Hz are slightly higher than those obtained from the frequency sweep. It is because the samples were first tested under the frequency sweep before the same samples were subsequently subjected to the temperature sweep. Such filler alignment could be induced during the previous measurement. Hence, from figure 5, the conductivity from the second and third measurement cycles is mostly independent of temperature, implying that the materials have their optimum conductivity after the first cycle. This suggests that the filler particles are aligned coherently along the longitudinal direction during

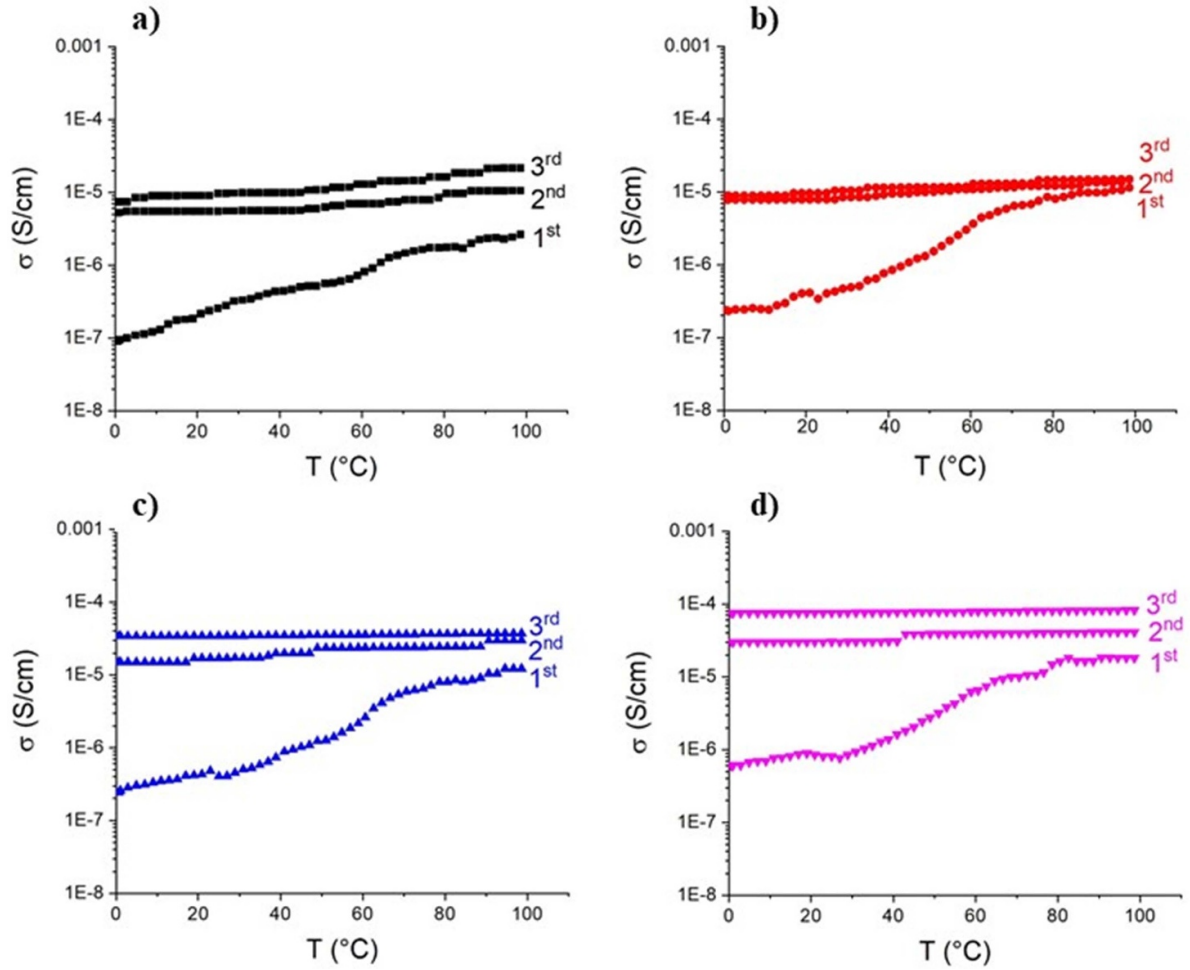

Figure 5. Electrical conductivity σ from a cyclic temperature sweep of the conductive compounds at 10 Hz and 0.35 and 0.25 MPa of static and dynamic stresses: C_{ref} (a), C_1 (b), C_2 (c), and C_3 (d).

the first measurement cycle and the acceleration of the charges mobility has a negligible effect on electrical conductivity in the following cycles.

According to the percolation theory, elastomers are conductive if filled with an amount of conductive fillers which exceeds a critical value, called percolation threshold. Higher surface area and aspect ratio of conductive particles implies a lower percolation threshold. Therefore, it is possible to conclude that the compound C_3 has the highest electrical conductivity compared to the other compounds as it contains the largest amount of nanofillers.

4.3. Ameliorating the interfacial adhesion between the piezoelectric polymer and conductive rubbers

PVDF is a fluoropolymer possessing low surface energy and is therefore very inert to chemical reactions. To prepare the piezoelectric patch with a sandwich-like configuration, the PVDF film and the conductive elastomer compound need to have good interfacial adhesion. Proper surface treatment of the PVDF film seems to be a good solution. An oxygen plasma treatment was used to generate the hydroxyl and carbonyl groups at the surface of the PVDF film [42], see figure 6(a). These functionalities are reactive towards further chemical species. The oxygen-modified PVDF film was silanised with 3-thiocyanatopropyltriethoxysilane, as shown in figure 6. The ethoxy groups of the silane can react with the active functionalities on the PVDF surface, by releasing ethanol as by-product. The other end group is a thiocyanate moiety, which introduces sulphur to the surface of the film, and participates in the vulcanisation reaction. This is expected to result in a strong adhesion between the interfaces [43].

To confirm the chemical modification of the PVDF surface, XPS spectroscopy was used to analyse the surface chemistry. Figure 6(a) shows the spectra of unmodified pure PVDF, plasma-treated PVDF and silanised PVDF using two different silanization times: 1 and 24 h. Table 4 summarises the atomic percentages of specific elements. The unmodified PVDF film cleaned with chloroform shows a clear fluorine (F) peak at 688 eV and two peaks of carbon (C) at 286–290 eV. The spectrum of unmodified PVDF shows a small peak of oxygen (O) at 533 eV, but the spectrum of the plasma-treated PVDF shows an increased concentration of oxygen at the surface, the amount is increased from 8.7 to 11.3 atomic percent. The silanisation reaction was proven by the decrease in fluorine and the increase in sulphur at the surface. As the silane is introduced

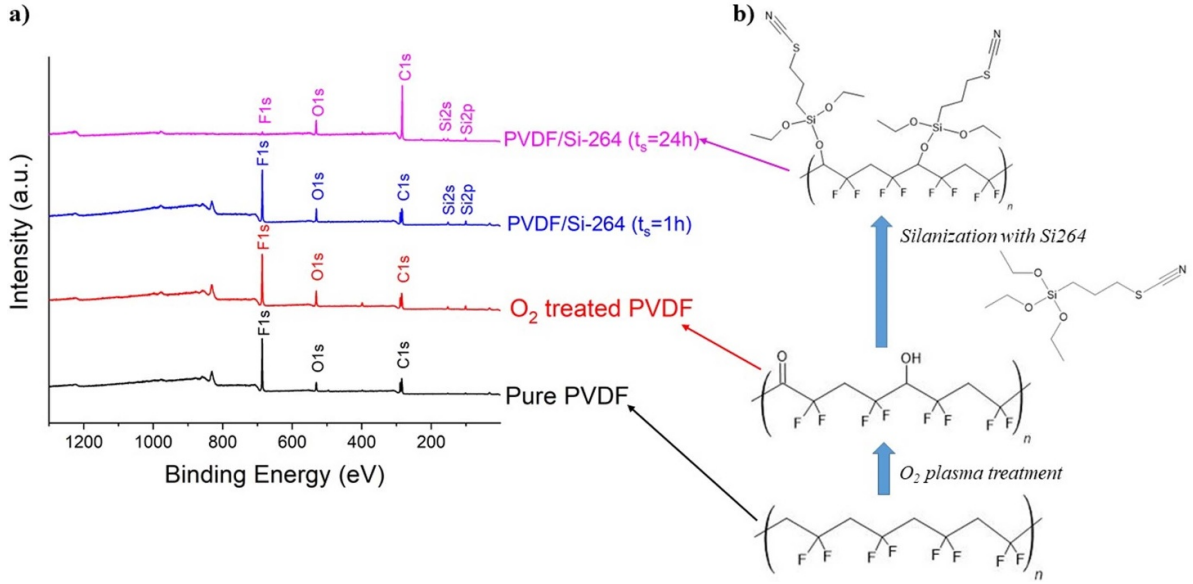

Figure 6. XPS spectra of unmodified PVDF film and after oxygen plasma-treatment PVDF and silanization for 1 h and 24 h with 3-thiocyanatopropyltriethoxysilane (Si-264) (a); and a proposed coupling mechanism (b).

Table 4. Atomic percentages of elements on the surface of PVDF films derived from XPS.

	Atomic percentage					
PVDFs treated with:	Carbon	Nitrogen	Oxygen	Fluorine	Silicon	Sulphur
Pure/untreated PVDF	54.2	1.4	8.7	33.2	2.1	—
Plasma modification	48.5	5.0	11.3	30.4	4.4	0.1[a]
3-thiocyanatopropyltriethoxysilane (1 h)	49.7	2.0	13.2	29.1	4.6	0.9
3-thiocyanatopropyltriethoxysilane (24 h)	77.8	2.9	11.0	1.1	4.3	2.9

[a] This data is doubtful and close to the detection limit of the machine.

to the surface, the amount of visible fluorine decreases, while the amount of sulphur increases. Increasing the silanization time from 1 to 24 h, the fluorine amount significantly decreases from 29.1 to 1.1 atomic percent. This confirms that the fluorine atoms are either replaced or covered by the silane coupling agent. Additionally, the amount of sulphur increases from 0.9 to 2.9 atomic percent, which also confirms the higher concentration of the modifying silane. This is expected to promote the chemical coupling to the conductive compounds. All the spectra of the different PVDF films contain a certain amount of silicon at the surface. This is probably due to contaminants that remained on the surface after the polymerization and poling process of the PVDF film.

The surface-treated PVDF films were then assembled with the electrically conductive rubber at 140 °C. During curing, the thiocyanate group is expected to react with rubber molecules, promoting the interfacial interaction between the two components. A T-peel test was carried out to measure the adhesive strength between the PVDF film and the reference compound C_{ref}. Figure 7(a) shows the forces used to peel the two components apart. A comparison between pure unmodified and 24 h silanised PVDF/C_{ref} was made. It is shown that a surface modification of the PVDF film by 3-thiocyanatopropyltriethoxysilane improves the adhesion between PVDF and the rubber. There is some standard deviation of the forces, either due to the peel test itself and/or not a fully homogeneous silanization on the PVDF surface.

Since the PVDF/C_{ref} piezoelectric patch has to withstand the rolling conditions of tyres, a time sweep analysis using a DMA was carried out. Figure 7(b) shows the results from the durability test of the piezoelectric sample under dynamic mechanical conditions with a double shear mode. Applying a constant dynamic strain during the measurements, a constant value of the dynamic force is observed over the testing time, meaning that the adhesion between the PVDF film and the conductive compound C_{ref} is stable. This gives a good validation that the adhesion between the components of the piezoelectric patch is durable.

4.4. Piezoelectric property of PVDF-based harvester

After optimisation of the electrically conductive compounds, the piezoelectric properties of the designed PEH were then studied. Figure 8 shows the power output derived from the harvesters as a function of frequency and temperature. It indicates that the output power increases at elevated frequencies, because there is a higher number of mechanical excitations to the material in a given time-span, activating the dipoles

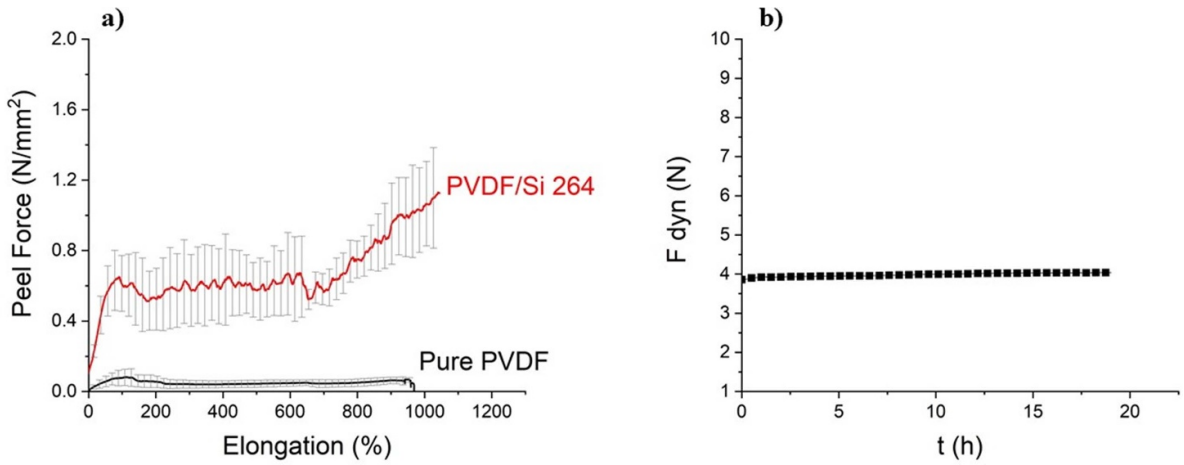

Figure 7. T-peel test in tensile machine (a); fatigue test in double shear mode in DMA at dynamic force F_{dyn} 10.5 N (b) of the piezoelectric harvester 24 h silanised PVDF/C_{ref}.

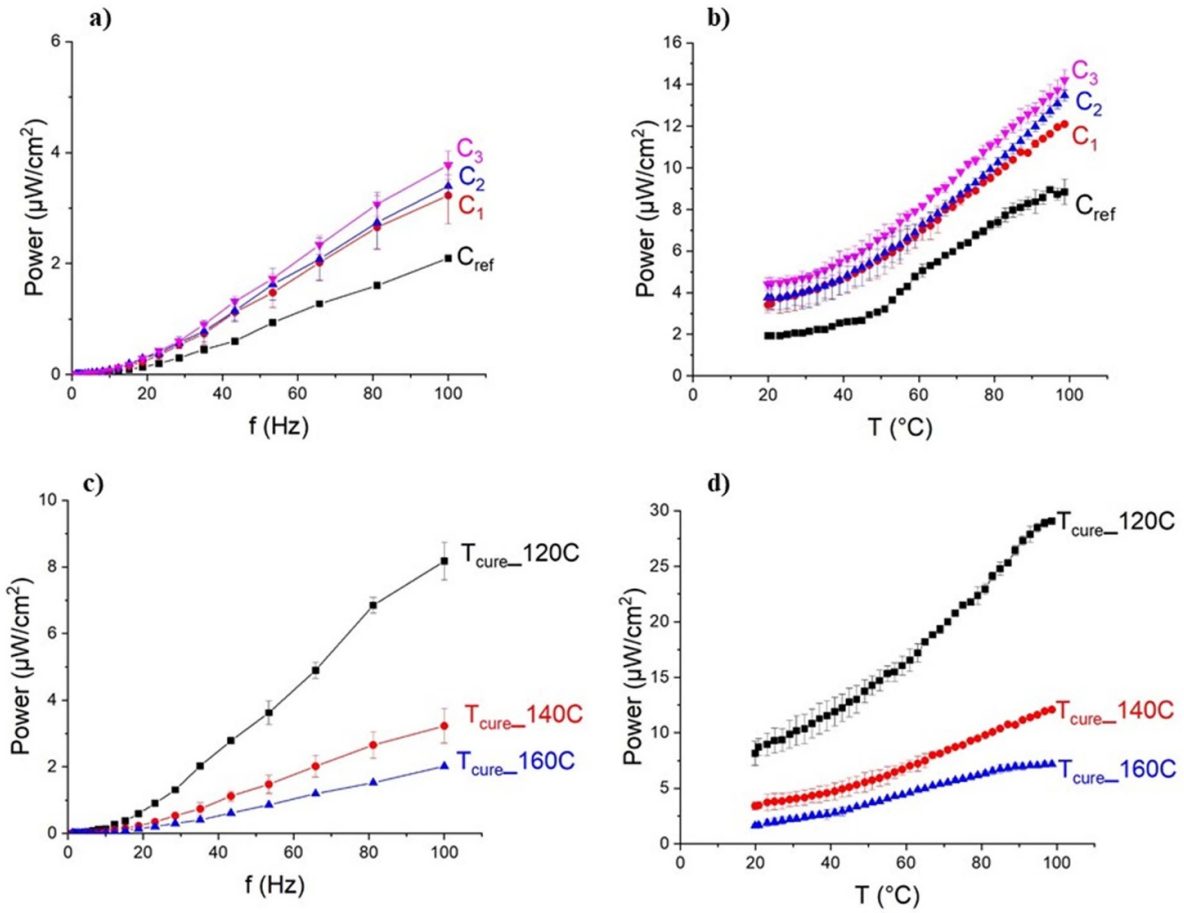

Figure 8. Output power from frequency sweep at 20 °C and temperature sweep at 100 Hz of piezoelectric patches with PVDF and conductive compounds C_{ref}, C_1, C_2 and C_3 (a) and (b) and PVDF/C_1 cured at 120 °C, 140 °C and 160 °C (c) and (d).

inside the PVDF film more frequently. The chemical adhesion between the piezoelectric film and the electrodes also plays an essential role on this characteristic. This adhesion creates a number of activation sites on PVDF surface. In this way, the current generated by the piezoelectric PVDF can flow in a more efficient manner, and the electrical conductivity of the electrodes is then crucial for the transferred current [44–47]. By increasing the temperature, figure 8(b), the generated power rises significantly because elevated temperatures increase the electrical conductivity as already shown in figure 4. Additionally, the piezoelectric effect increases with increasing temperature due to the higher mobility of dipoles in

the PVDF film, resulting in higher power output. The piezoelectric patch within the conductive compound C_3 with 6 wt% of carbon nanotubes masterbatch provides most generated electricity due to the highest value of conductivity of C_3. The generated electrical power of the piezoelectric patch PVDF/C_3 varies between 10 and 14 μW cm^{-2} at 80 °C–100 °C, which is the operating temperature of rolling tyres.

For PVDF films, the maximum operating temperature at which the films can still generate electricity is usually 100 °C depending on how the films are processed [48]. According to the information from the supplier, the PVDF film investigated in this study has still more than 50% piezoelectric performance at 120 °C. In figures 8(a) and (b), the piezoelectric samples were vulcanised at 140 °C. To study more in-depth the effect of vulcanisation temperature, the PVDF film was assembled into the piezoelectric patch with the conductive compound C_1 and also cured at 120 °C and 160 °C. Figures 8(c) and (d) show the output power from the piezoelectric samples based on PVDF/C_1 cured at 120 °C, 140 °C and 160 °C. The curing temperature has a strong influence on the output power generated by the piezoelectric samples. From the frequency dependence test, figure 8(c), the sample cured at 120 °C exhibits the highest power at 100 Hz, which is around 65% higher than for the sample cured at 140 °C and around 75% higher than for the sample cured at 160 °C. Similarly, in figure 8(d), the sample vulcanised at 120 °C produced a higher power of around 68% compared to the sample cured at 140 °C and around 82% higher than the sample cured at 160 °C.

4.5. Interfacial adhesion between the conductive compound and inner liner

To investigate the adhesion performance of the piezoelectric patch to the inner liner of a tyre, two approaches can be considered, to co-cure the two components or to use a suitable glue. The first option introduces some problems with the curing temperature of a tyre, which is in the range of 160 °C–180 °C. These temperatures will lead to a significantly reduced power output of the patch, as shown in figure 8. Therefore, the second option was taken for the trial. The durability of the sample prepared by combining layers of conductive and inner liner compounds was investigated using a DMA. The patch of the conductive compound added with 6 wt% of carbon nanotube masterbatch (C_3), with a width of 10 mm and a thickness of 2 mm, was glued to the inner liner masterbatch (C_{IL}) with the same dimensions. Subsequently, the sample was analysed for its durability with a double shear fatigue test at 2% dynamic strain, and the obtained results are shown in figure 9. The result shows a good stability of the sample over a measurement time of 20 h. Therefore, the glue used between these two components is potentially effective for this system.

4.6. Validation and evaluation of the prototyped PEH patch

To validate the processability of the designed system, all experimental results were considered in relation to the actual application of the prototype in a tyre. In figure 10, the output

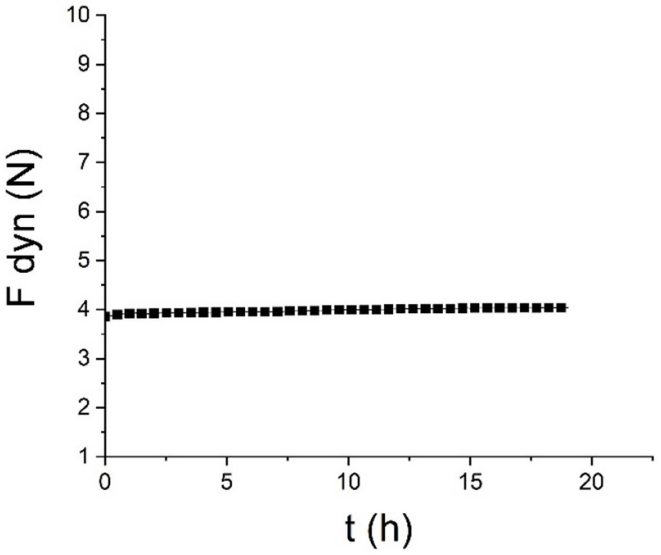

Figure 9. Fatigue test of two individual samples prepared by combining two layers of conductive and inner liner compounds using a time sweep analysis with a double shear mode at 2% dynamic strain (and dynamic force F_{dyn} of 4 N).

power generated by the harvester, composed of PVDF film and the elastomeric conductive compounds with 6 wt% of carbon nanotubes masterbatch and vulcanised at 120 °C, is reported. Based on these results, it is clear that this piezoelectric patch generates more electricity with increasing frequency and temperature again. These values were taken for a calculation linking the lab conditions to the actual rolling conditions of the reference tyre. At 100 Hz and 90 °C in a DMA, the output power from the piezoelectric patch developed in this work produced 28 μW cm^{-2}. To ensure that a sufficient amount of energy is supplied to the reference TPMS sensor, which needs 28 mW, the piezoelectric patch should have surface area of 1000 cm^2. Therefore, the patch can be installed inside a tyre as a continuous layer along the circumference, ca. 200 cm.

The piezoelectric patch can also have a smaller area, taking into account that TPMS measures the pressure every 10 or 100 s. This allows the possibility to have a TPMS with lower power consumption, as well as safe driving. For collecting the measurement points every 10 or 100 s, the TPMS requires a power of 2.8 mW or 0.28 mW, respectively. As a result, the area of the piezoelectric patch to power the TPMS can be decreased resulting respectively in 100 and 10 cm^2. Consequently, the patch must be a square strip attached to the inner liner with dimensions of 10 $\times$ 10 cm^2 for a sampling rate of 0.1 measurement points s^{-1} or of 3.2 $\times$ 3.2 cm^2 for a sampling rate of 0.01 points s^{-1}.

Another important point to mention concerns the adhesion of the PEH to the inner liner of a tyre. In the present work, it was considered to prepare the PEH first and then adhere it to the inner liner. This two-steps fabrication of PEH implies a small-sized harvester due to higher output power, but a slightly more complex manufacturing process. The other approach is to vulcanise the PEH components directly onto the inner liner of the tyre at 160 °C. This would imply an

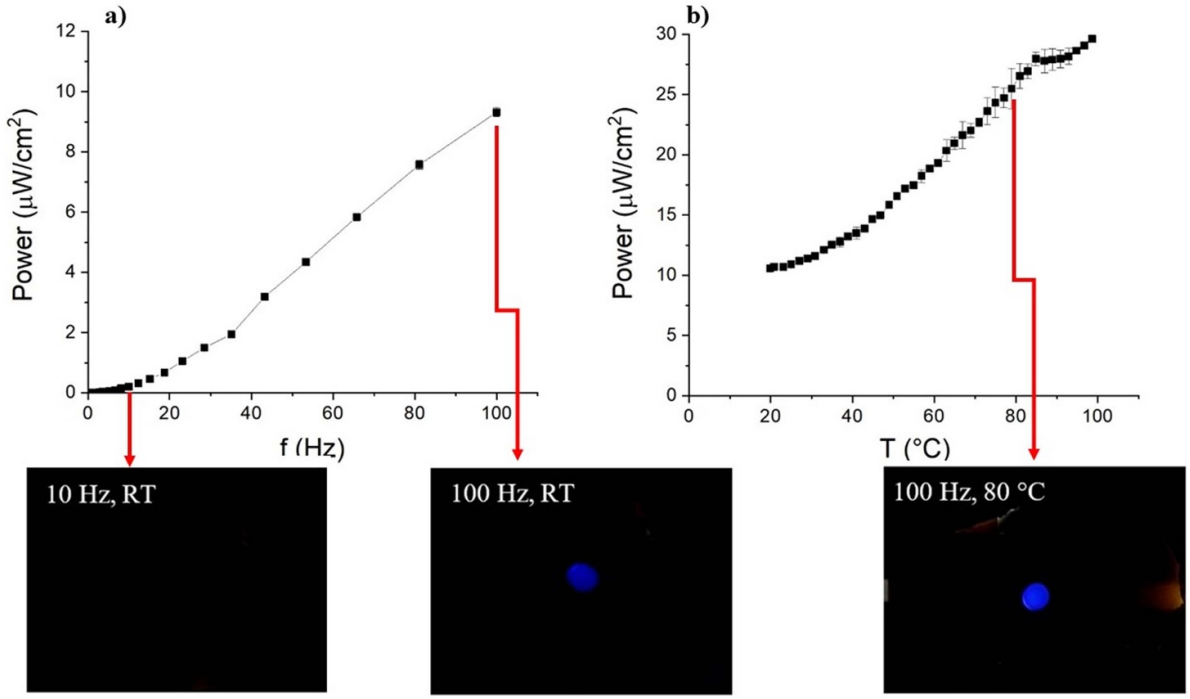

Figure 10. Power output generated by the prototyped PEH analysed under frequency sweep at 20 °C (a); temperature sweep at 100 Hz (b); images of LED light during DMA measurements at 10 and 100 Hz and room temperature (RT) and 80 °C.

easier manufacturing process but 4-times lower output power and in turn a 4-times larger patch (as shown in figure 8(d)). This aspect of the current design depends on factors like customer demands and the specific TPMS device.

Confirmation of the efficiency of the designed prototype to generate electricity is the evidence that this piezoelectric patch is capable of powering a light-emitting diode (LED) bulb. This experiment was set by connecting the LED to the piezoelectric system, using the same measurement setup as discussed in section 4.3. The piezoelectric patch was installed in a DMA and coupled to a bridge rectifier which converts the AC output into DC input for the LED. A blue LED (TessaTronic, Hengelo, the Netherlands) was able to be powered by a voltage of around 2.0 V. Figure 10 shows the images of the LED powered with different frequencies: 10 and 100 Hz; and temperatures: room temperature and 80 °C. The LED light becomes more intense with increasing temperature and frequency. At 10 Hz and room temperature, the LED could not be powered, but at 100 Hz and 80 °C it gave the brightest light. Therefore, this result provides a clear validation of the performance of the piezoelectric patch designed in the present work.

5. Conclusions

A flexible PEH was developed. The designed piezoelectric patch includes two components configured in a sandwich structure: a piezoelectric polymer film inserted in between two layers of conductive rubber compound. The selected piezoelectric polymer was a PVDF film with a thickness of 0.1 mm with high piezoelectric coefficient and acceptable flexibility. A conductive rubber compound filled with CB was employed because of its high elasticity and good adherence to tyre compounds, in particular to the inner liner. The electrical conductivity of the compound can significantly be enhanced using a SWCNT masterbatch with TDAE oil as base. 6 wt% of the masterbatch is the minimum amount of nanofillers which is required to have an elastomeric compound with a conductivity of 10^{-4} S cm^{-1}. The conductivity of the compounds tends to be constant after the first temperature sweep analysis, since the particles of CB and carbon nanotubes are well aligned, forming a conductive networking path throughout the matrix.

To fabricate all into a flexible energy harvester patch, a surface treatment of the PVDF film using a silane coupling agent was required to enable the adhesion between the film and the conductive elastomer. XPS analyses confirm that the surface modifications of the PVDF film by an oxygen-plasma treatment followed by a silanisation reaction via a thiocyanate silane were successful. The adhesion strength between the PVDF film and the conductive compound was enhanced during T-peel test and it was durable during a time-sweep dynamic mechanical analysis simulating the actual conditions of a rolling tyre.

Finally, the surface-treated PVDF was cured in between two layers of the elastomeric conductive compound at 120 °C. Under the assumption of a reference passenger car, the piezoelectric patch with dimensions of 10 × 10 cm^2 can power a TPMS device that requires 28 mW of electricity. Assembly of this harvester to the inner liner of a tyre can be done by glueing it with a silicone adhesive.

Data availability statement

The data that support the findings of this study are available upon reasonable request from the authors.

Acknowledgments

The authors acknowledge the company partner Apollo Tyres Global R&D Ltd for financially supporting the project and providing the rubber compounds as well as the tyre data.

Conflict of interest

The authors declare that they have no known competing financial interests or personal relationships that could have appeared to influence the work reported in this paper.

ORCID iDs

Carmela Mangone https://orcid.org/0000-0002-6765-0556
Wisut Kaewsakul https://orcid.org/0000-0002-8369-4575

References

[1] Shaikh F K and Zeadally S 2016 Energy harvesting in wireless sensor networks: a comprehensive review *Renew. Sustain. Energ. Rev.* **55** 1041–54
[2] Kim H, Tadesse Y and Priya S 2009 Piezoelectric energy harvesting *Energy Harvesting Technologies* (Boston, MA: Springer US) pp 3–39
[3] Löhndorf M and Lange T 2013 MEMS for automotive tire pressure monitoring systems *MEMS for Automotive and Aerospace Applications* (Philadelphia, PA: Woodhead Publishing) pp 54–77
[4] Bowen C R and Arafa M H 2015 Energy harvesting technologies for tire pressure monitoring systems *Adv. Energy Mater.* **5** 1401787
[5] Matsuzaki R and Todoroki A 2008 Wireless monitoring of automobile tires for intelligent tires *Sensors* **8** 8123–38
[6] Wu B, Fang Y and Deng L 2019 Summary of energy collection application in vehicle tire pressure monitoring system *4th Int. Conf. on Automation, Control and Robotics Engineering* (*Shenzhen*) vol 19 pp 1–6
[7] Kubba A E and Jiang K 2014 A comprehensive study on technologies of tyre monitoring systems and possible energy solutions *Sensors* **14** 10306–45
[8] Yang Z, Zhou S, Zu J and Inman D 2018 High-performance piezoelectric energy harvesters and their applications *Joule* **2** 642–97
[9] Anton S R and Sodano H A 2007 A review of power harvesting using piezoelectric materials (2003–2006) *Smart Mater. Struct.* **16** R1–R21
[10] Toghi Eshghi A, Lee S, Lee H and Kim Y-C 2016 Parameter study and optimization for piezoelectric energy harvester for TPMS considering speed variation *Proc. SPIE* **9806** 1–19
[11] Lee J, Kim S, Oh J and Choi B 2012 A self-powering system based on tire deformation during driving *Int. J. Automot. Technol.* **13** 963–9
[12] Al-Najati I A H, Chan K W and Pung S Y 2022 Tire strain piezoelectric energy harvesters: a systematic review *Int. J. Power Electron. Drive Syst.* **13** 444–59
[13] Chilabi H J, Salleh H, Al-Ashtari W, Supeni E E, Abdullah L C, As'arry A B, Rezali K A M and Azwan M K 2021 Rotational piezoelectric energy harvesting: a comprehensive review on excitation elements, designs, and performances *Energies* **14** 3098
[14] Al-Yafeai D, Darabseh T and Mourad A-H 2020 A state-of-the-art review of car suspension-based piezoelectric energy harvesting systems *Energies* **13** 2336
[15] Keck M 2007 A new approach of a piezoelectric vibration-based power generator to supply next generation tire sensor systems *Proc. IEEE Sensors* pp 1299–302
[16] Zheng Q, Tu H, Agee A and Xu Y 2009 Vibration energy harvesting device based on asymmetric air-spaced cantilevers for tire pressure monitoring system *PowerMEMS* (*Washington, DC*) pp 403–6
[17] Elfrink R *et al* 2011 Shock induced energy harvesting with a MEMS harvester for automotive applications *2011 Int. Electron Devices Meeting* (*Washington, DC*) pp 677–80
[18] Mak K H, McWilliam S and Popov A A 2013 Piezoelectric energy harvesting for tyre pressure measurement applications *Proc. Inst. Mech. Eng.* D **227** 842–52
[19] Jousimaa O J, Xiong Y, Niskanen A J and Tuononen A J 2016 Energy harvesting system for intelligent tyre sensors *2016 IEEE Intelligent Vehicles Symp. (IV)* (*Gothenburg*) pp 578–83
[20] Zhu B, Han J, Zhao J and Deng W 2017 Practical design of an energy harvester considering wheel rotation for powering intelligent tire systems *J. Electron. Mater.* **46** 2483–93
[21] Makki N and Pop-Iliev R 2011 Piezoelectric power generation in automotive tires *Smart Materials, Structure & NDT in Aerospace* (*Montreal*)
[22] Makki N and Pop-Iliev R 2011 Pneumatic tire-based piezoelectric power generation *Proc. SPIE* **7977** 1–10
[23] Van den Ende D A, van de Wiel H J, Groen W A and van der Zwaag S 2011 Direct strain energy harvesting in automobile tires using piezoelectric PZT–polymer composites *Smart Mater. Struct.* **21** 015011
[24] Tang Q C and Li X X 2012 Non-contact frequency-up-conversion energy harvester for durable & broad-band automotive TPMS application *2012 IEEE 25th Int. Conf. on Micro Electro Mechanical Systems (MEMS)* (*Paris*) pp 1273–6
[25] Wu X, Parmar M and Lee D W 2014 A seesaw-structured energy harvester with superwide bandwidth for TPMS application *IEEE/ASME Trans. Mechatron.* **19** 1514–22
[26] Fan H *et al* 2022 Enhanced ferroelectric and piezoelectric properties in graphene-electroded $Pb(Zr,Ti)O_3$ thin films *ACS Appl. Mater. Interfaces* **14** 17987–94
[27] Zheng H, Zhang H, Wen P and He D 2022 Flexible piezoelectric energy harvester based on graphene macro-film electrode enabled by exploiting auxetic mechanical property *Mater. Lett.* **318** 132165
[28] Cheong H-G, Kim J-H, Song J-H, Jeong U and Park J-W 2015 Highly flexible transparent thin film heaters based on silver nanowires and aluminum zinc oxides *Thin Solid Films* **589** 633–41
[29] Kim T, Cui Z, Chang W-Y, Kim H, Zhu Y and Jiang X 2020 Flexible 1-3 composite ultrasound transducers with silver-nanowire-based stretchable electrodes *IEEE Trans. Ind. Electron.* **67** 6955–62
[30] Renteria A *et al* 2022 Direct ink write multi-material printing of PDMS-BTO composites with MWCNT electrodes for flexible force sensors *Flex. Print. Electron.* **7** 015001

[31] Donnet J-B, Bansal R C and Wang M-J 1993 *Carbon Black: Science and Technology* 2nd edn (Boca Raton, FL: CRC Press Taylor & Francis) (https://doi.org/10.1201/9781315138763)
[32] Spahr M E and Rothon R 2016 Carbon black as a polymer filler *Polymers and Polymeric Composites: A Reference Series* (Berlin: Springer) pp 1–31
[33] Kochervinskii V V 1999 Ferroelectricity of polymers based on vinylidene fluoride *Russ. Chem. Rev.* **68** 821–57
[34] Mangone C, Klein-Gunnewiek M and Reuvekamp L A E M 2021 *US Patent* WO/2021/052957
[35] Bhagavatheswaran E S, Stöckelhuber K W, Vaikuntam S R, Wießner S, Pötschke P, Heinrich G and Das A 2018 Time and temperature dependent piezoresistive behavior of conductive elastomeric composites *Rubber Chem. Technol.* **91** 651–67
[36] Yamaguchi K, Busfield J J C and Thomas A G 2003 Electrical and mechanical behavior of filled elastomers I. The effect of strain *J. Polym. Sci.* B **41** 2079–89
[37] Khameneifar F, Arzanpour S and Moallem M 2013 A piezoelectric energy harvester for rotary motion applications: design and experiments *IEEE/ASME Trans. Mechatron.* **18** 1527–34
[38] Rodgers B and Waddell W 2005 Tire engineering *Science and Technology of Rubber* 3rd edn (Burlington, VT: Academic) ch 14, pp 619–61, I–II
[39] Bhagavatheswaran E S 2019 Exploring the piezoresistive characteristics of solution styrene butadiene rubber composites under static and dynamic conditions—a novel route to visualize filler network behavior in rubbers *PhD Thesis* Technische Universität, Dresden
[40] Meier J G and Klüppel M 2008 Carbon black networking in elastomers monitored by dynamic mechanical and dielectric spectroscopy *Macromol. Mater. Eng.* **293** 12–38
[41] Nakaramontri Y, Pichaiyut S, Wisunthorn S and Nakason C 2017 Hybrid carbon nanotubes and conductive carbon black in natural rubber composites to enhance electrical conductivity by reducing gaps separating carbon nanotube encapsulates *Eur. Polym. J.* **90** 467–84
[42] Correia D M, Ribeiro C, Sencadas V, Botelho G, Carabineiro S A C, Ribelles J L G and Lanceros-Méndez S 2015 Influence of oxygen plasma treatment parameters on poly(vinylidene fluoride) electrospun fiber mats wettability *Prog. Org. Coat.* **85** 151–8
[43] Mangone C, Klein-Gunnewiek M, Reuvekamp L A E M, Kaewsakul W and Blume A 2021 *US Patent* WO/2021/052951
[44] Wathore N N, Rawal B, Dixit P, Mandave S, Praveenkumar B and Rajan K M 2019 Effect of silver electrode annealing temperature on electrical properties of sodium potassium niobate based ceramics *J. Electron. Mater.* **48** 845–52
[45] Baik K, Park S, Yun C and Park C H 2019 Integration of polypyrrole electrode into piezoelectric PVDF energy harvester with improved adhesion and over-oxidation resistance *Polymers* **11** 1071
[46] Ahn T-C, Hong H-S, Kim -S-S and Hwang H-Y 2022 Improvement of adhesion characteristics of copper electrodes on polyvinylidene fluoride films using bovine serum albumin *Int. J. Adhes. Adhes.* **112** 103025
[47] Elyashevich G K, Dmitriev I Y and Rozova E Y 2021 Electroconducting polypyrrole coatings as an electrode contact material on porous poly(vinylidene fluoride) piezofilm *Polym. Sci.* A **63** 45–53
[48] Bauer S and Bauer F 2008 Piezoelectric polymers and their applications *Piezoelectricity: Evolution and Future of a Technology* (Berlin: Springer) pp 157–77